Analytica Chimica Acta 1213 (2022) 339960

Contents lists available at ScienceDirect

Analytica Chimica Acta

journal homepage: www.elsevier.com/locate/aca

High-performance biosensor using a sandwich assay via antibody-conjugated gold nanoparticles and fiber-optic localized surface plasmon resonance

Hyeong-Min Kim, Hyo-Jun Kim, Jae-Hyoung Park **, Seung-Ki Lee *

Department of Electronics and Electrical Engineering, Dankook University, Yongin, 16890, Republic of Korea

HIGHLIGHTS

- A sandwich-type localized surface plasmon resonance based on the optical fiber was developed.
- Sandwich structure by gold nanoparticles amplified outputs in biosensing.
- High sensitivity was achieved with the limit of detection of 6.6 fg/mL.
- Selectivity with other antigens was confirmed with fair interference.
- Antigen levels measured by commercial kit and our method were compared.

GRAPHICAL ABSTRACT

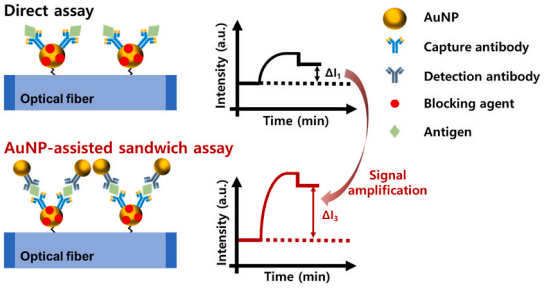

ARTICLE INFO

Keywords:
Antibody-gold nanoparticle conjugate
Biosensor
Localized surface plasmon resonance
Microfluidic chip
Optical fiber
Sandwich immunoassay

ABSTRACT

For real-time and high-sensitivity analysis of low-concentration targets, a sandwich immunoassay using second antibody-second gold nanoparticle (2nd Ab-2nd AuNP) conjugates was combined with fiber-optic localized surface plasmon resonance (FO LSPR). An FO LSPR format was constructed by immobilizing AuNPs on a fiber-optic cross-section for compactness, portability, and ease of handling. In addition, it was combined with a microfluidic system to ensure reproducibility and reliability of measurements. A detection limit of 97.6 fg/mL (148 aM) was obtained for thyroglobulin (Tg) without a sandwich assay. The detection limit was enhanced by approximately 15 times (6.6 fg/mL, 10 aM) when a sandwich strategy was performed with a 2nd Ab-2nd AuNP signal amplifier to further improve the responsivity. Additionally, the good selectivity of the proposed method was confirmed against the unpaired antigen. To evaluate its practical applicability in the field, an FO LSPR biosensor boosted with a sandwich assay using antibody-functionalized AuNPs was applied to detect Tg contained in patient serum, and the results were compared and verified with those of a commercial radioimmunoassay kit. Based on the above results, the signal-enhancing immunoassay with FO LSPR will contribute to the development of optical biosensors for early diagnosis and preventive applications.

* Corresponding author.
** Corresponding author.
E-mail addresses: parkjae@dankook.ac.kr (J.-H. Park), skilee@dankook.ac.kr (S.-K. Lee).

https://doi.org/10.1016/j.aca.2022.339960
Received 15 March 2022; Received in revised form 16 May 2022; Accepted 17 May 2022
Available online 20 May 2022

1. Introduction

For successful treatment of, and full recovery from, diseases via early detection, technology that can rapidly identify small quantities of targets is required [1,2]. With the convergence of technologies across multiple fields, traditional test methods that require several stages and skilled practitioners have gradually progressed with the aid of varied and simplified equipment, and high-sensitivity techniques with excellent performance have emerged [3–5]. However, highly sensitive detection using simple approaches remains actively sought after [6–8]. Therefore, we intend to improve responsiveness by introducing a simple sensing platform. The principle used in protein detection is known as localized surface plasmon resonance (LSPR), which is a representative method for label-free detection in the optical field [9–11]. LSPR quantifies proteins through refractive index changes and is considered a promising biosensor with the advantage of real-time measurement of the binding of biomolecules to nanostructures [12–14]. LSPR sensors are also easy to fabricate because they can be configured with only metal nanoparticles and are highly sensitive to changes in the refractive index of the surrounding environment owing to the high surface-to-volume ratio of the nanoparticles [15–17]. Among the LSPR configurations, fiber-optic LSPR (FO LSPR) provides improved sensing capability for various applications with advantages such as small size, low cost, simple fabrication, and ease of handling [18–20]. The FO LSPR biosensor is fabricated by forming metal nanoparticles on the core of an optical fiber and fixing a receptor thereon. The sensing mechanism is based on phase matching between the waveguide mode of the optical fiber and the localized surface plasmon mode. It can identify changes in the resonance peak and intensity generated by the refractive index variation of the sensing region with antigen binding [21,22].

Biosensor analysis methods are broadly classified into three categories: direct assays, sandwich assays, and competitive assays [23]. Among these, the sandwich assay can achieve relatively high susceptibility, accuracy, and specificity [24]. The sandwich method is a model in which the antigen is located between the capture and detection antibodies. In other words, capture antibodies are first adsorbed onto the transducer surface, then antigen binding is induced, and finally, the detection antibodies are tied to the antigen. Various markers such as enzymes, fluorescent dyes, and redox molecules are labeled on the detection antibodies for signal recognition and amplification [25–28]. However, they have limitations in terms of sensitivity and specificity in sample analyses owing to the influence of temperature, pH, and substrate [29,30]. LSPR is a label-free method that can detect antigen binding using only capture antibodies (first-adsorbed antibodies) through refractive index changes (Scheme 1A). In addition, distinct markers are not required, even when the detection antibodies (second-adsorbed antibodies) are sandwiched (Scheme 1B). However, to enhance the LSPR output by target immobilization, research using complexes that combine secondary metal nanoparticles with detection antibodies has been reported [31,32]. Nanoparticles are non-toxic markers and have the potential for surface modification, stability, and acceleration of LSPR susceptibility [33–36]. In particular, gold nanoparticle (AuNP) was adopted with biocompatibility, ease synthesis, high conductivity, steadiness in oxidizing environments [37–39]. Therefore,

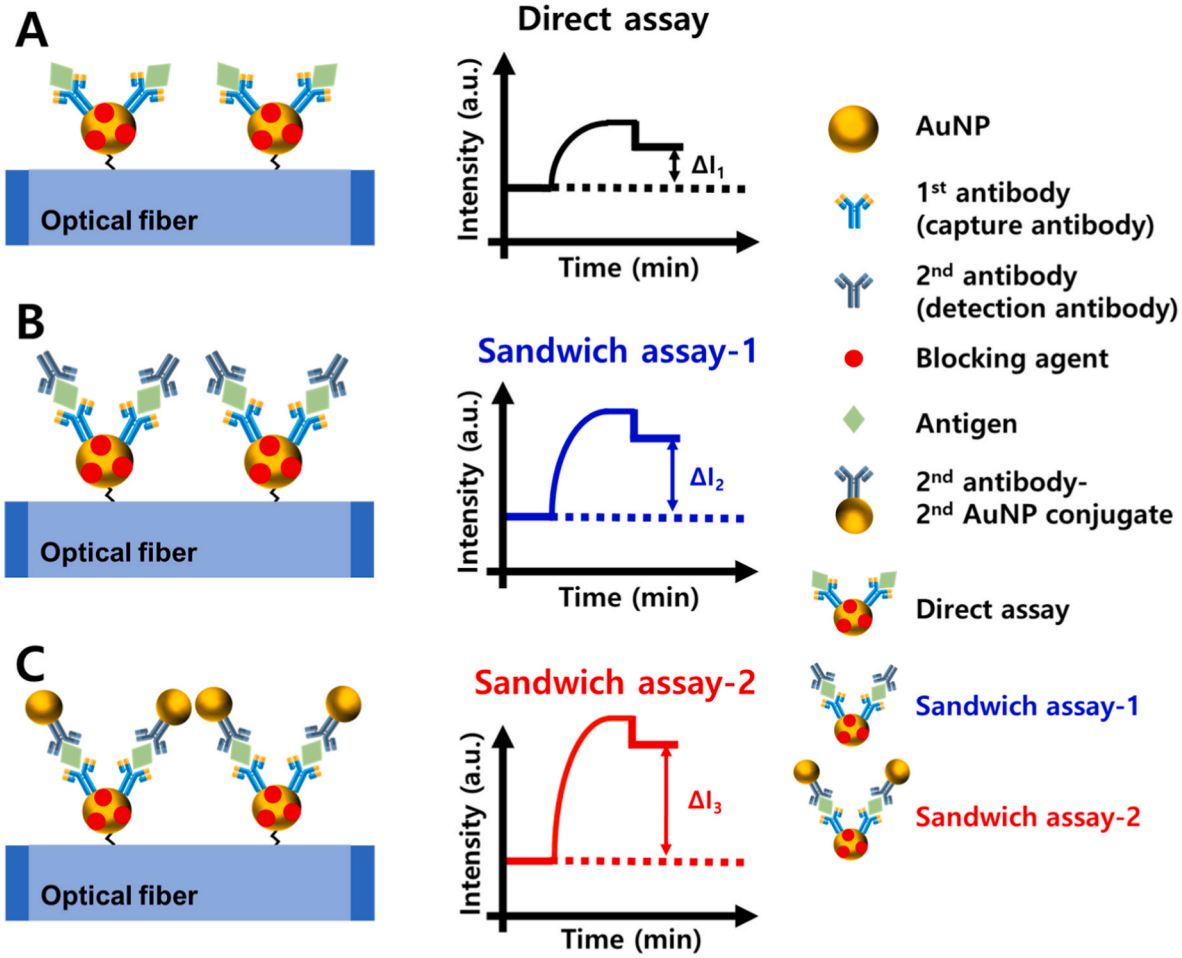

Scheme 1. Various analysis methods for immunoassays. (A) Direct assay, (B) sandwich assay with 2nd antibody (sandwich assay-1), and (C) sandwich assay using 2nd Ab-2nd AuNP conjugates (sandwich assay-2).

we propose a sandwich immunoassay that uses second antibody-second AuNP (2nd Ab-2nd AuNP) conjugates (detection antibody-functionalized AuNPs) to improve the detection limit of FO LSPR (Scheme 1C). 2nd Ab-2nd AuNP compounds, which are sequentially introduced on the antigens, generate an extra LSPR signal on the fiber-optic surface and can also induce coupling with previously fixed nanoparticles. These scenarios support the magnification of the output by antigen sensing [40]. To the best of our knowledge, FO LSPR biosensors using antibody-conjugated AuNPs have not been previously developed.

In this study, a sandwich-type LSPR sensor based on an optical fiber for signal amplification was developed as a highly sensitive and simple biosensor. Amplification efficiency was enhanced by marking the AuNPs with detection antibodies. An FO LSPR biosensor was easily fabricated by attaching spherical AuNPs onto an optical fiber and adsorbing antibodies to the Au surface. For reproducibility and reliability of the measurement results, a microfluidic chip was applied to the FO LSPR biosensor, which is beneficial for reactivity with the target, sample consumption, and convenient measurement [41]. The biosensor chip determines different concentrations of antigen with the direct assay, a sandwich assay using only a 2nd antibody (sandwich assay-1), and a sandwich assay using 2nd Ab-2nd AuNP conjugates (sandwich assay-2) (Scheme 1). To validate the selectivity of our method, non-specific binding was checked using an unmatched antigen. Finally, its value as a practical tool for disease diagnosis was proved using a serum sample. This approach can contribute to early detection by identifying small quantities of analytes.

2. Material and methods

2.1. Chemicals and reagents

Sulfuric acid (H_2SO_4, 95%) and hydrogen peroxide (H_2O_2, 34.5%), which are used to clean the optical fiber and introduce a self-assembled monolayer (SAM) on the surface, isopropanol (C_3H_8O, 99.9%) for dilution of 3-aminopropyldimethylethoxysilane (APMES, $C_7H_{19}NOSi$, 97%), sodium citrate dihydrate ($C_6H_5Na_3O_7{\cdot}2H_2O$, 99%), which is added as a reducing agent in the synthesis of AuNPs, glycerol ($C_3H_8O_3$, 99%) for refractive index solutions, and buffer solution pH 5, 6, 7 at 25 °C were purchased from Daejung Chemicals and Metals, Republic of Korea. To form an SAM containing amine groups on the fiber-optic end-face, APMES was supplied by Gelest, USA. Gold (III) chloride trihydrate ($HAuCl_4{\cdot}3H_2O$, 99%), used in the preparation of Au colloid, bovine serum albumin (BSA, ≥98%), which is applied to a blocking agent to prevent non-specific binding, phosphate buffered silane (PBS, 0.01 M phosphate buffer, 0.0027 M potassium chloride, 0.137 M sodium chloride, pH 7.4), which is used as a buffer for immunoassays, and potassium carbonate (CK_2O_3, ≥98%) for pH adjustment of the Au colloidal solution were obtained from Sigma Aldrich, USA. Thyroglobulin (Tg), capture and detection anti-Tg antibodies were provided by Shin Jin Medics, Republic of Korea. Ferritin (human spleen, P1450), used to check the selectivity of the Tg biosensor, was obtained from Biovision, USA. Polydimethylsiloxane (PDMS) was purchased from Sewang High Tech, Republic of Korea for the fabrication of the microfluidic channel.

2.2. FO LSPR sensor fabrication

Fig. 1 illustrates the manufacturing process of the FO LSPR sensor. In the preparation stage, a multimode optical fiber (FG105LCA, Thorlabs, USA) with core and cladding diameters of 105 μm and 125 μm was cut to 15 cm. To prevent damage to the jacket during the chemical dipping processes, 3 cm of the jacket was removed from one end with a stripper (HT-S144H, KFT, Taiwan). Sequentially, it was vertically cleaved (S326, OFS Fitel, USA) to obtain a precise end-face. After the fiber-optic trim, they were first treated with piranha solution (4:1 vol ratio of sulfuric acid to hydrogen peroxide) for 20 min to form hydroxyl groups (Fig. 1A). Second, 5% APMES diluted in isopropanol was used to generate an SAM on the hydrophilic surface (Fig. 1B). The reaction time was set at 90 min. The SAM using APMES consisted of head groups with Si and functional groups with amine creates silanol bonds with hydroxyl groups on the fiber-optic surface. That is, the substrate was positively charged by amine functionalization, which was applied to immobilize negatively charged AuNPs [42]. Finally, the optical fiber was dipped in the Au colloidal solution, which was arranged with the citrate reduction method by mixing 0.1% gold (III) chloride trihydrate and 1% sodium citrate dihydrate in a ratio of 100:1 (Fig. 1C). AuNP concentration was 3.1×10^{10} particles/mL. The consumed time was 60 min, and the chemicals were dissolved in distilled (DI) water. The Au surface was negatively charged by citrate and electrostatically bound to the amine groups. Nanoparticles of approximately 55 nm were produced by the above AuNP synthesis conditions, which was selected as the optimal size to ensure the reproducibility and reliability of measurements in our optical system (including the optical fiber, light source, and spectrometer) based on a previous study [43], though AuNPs with a smaller diameter can exhibit greater sensitivity [44]. The FO LSPR sensors were integrated with microfluidic chips. The manufacturing process of the PDMS channel and the combination procedures with FO LSPR are described in Fig. S1. The microfluidic chip was joined to avoid contamination from the external environment and evaporation of samples at the sensor surface [45]. Fig. 1D shows a field emission scanning electron microscope (FE-SEM, S-5200, Hitachi, Japan) image of the fiber-optic end surface after fixing the AuNPs. The average size of the particles was 53.6 ± 2.1 nm with an even distribution. In Fig. S2, energy dispersive X-ray analysis of spherical AuNPs onto an optical fiber was performed to verify the composition of the particles.

2.3. Optical measurement setup

The measurement environment is shown in Fig. 2A, which consists of a white light source (HL-2000-LL, Ocean Optics, USA), a spectrometer (SM245, Korea Spectral Products, USA), and a 2 × 1 coupler (coupling ratio of 50:50, Thorlabs). The two ports of the 2 × 1 coupler were linked to a spectrometer via a subminiature version A connector and a light source with a fiber channel and physical contact cable, respectively. One port without a connector was spliced (A-80S, Walfront, China) using the FO LSPR sensor. Light from the source reached the sensor surface by total internal reflection in the optical fiber and excited the AuNPs. The scattering signal generated in the AuNPs was again collected in the optical fiber and recorded using the spectrometer, and the samples were

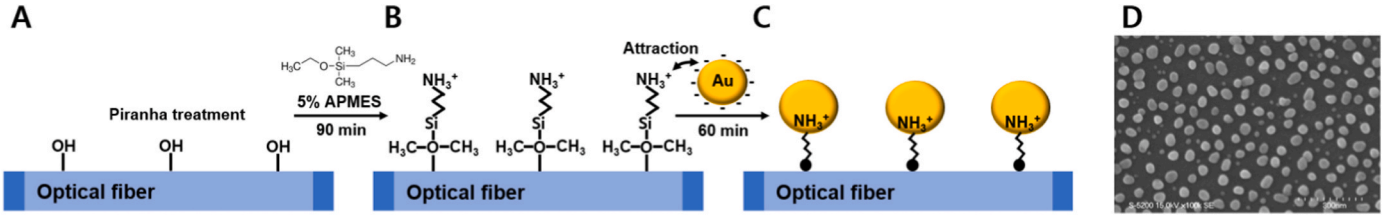

Fig. 1. Fabrication steps for the FO LSPR sensor: (A) hydroxyl group functionalization with piranha solution, (B) SAM formation with amine groups, (C) electrostatic attachment of AuNPs, and (D) FE-SEM photograph of the tip-end of the FO LSPR sensor.

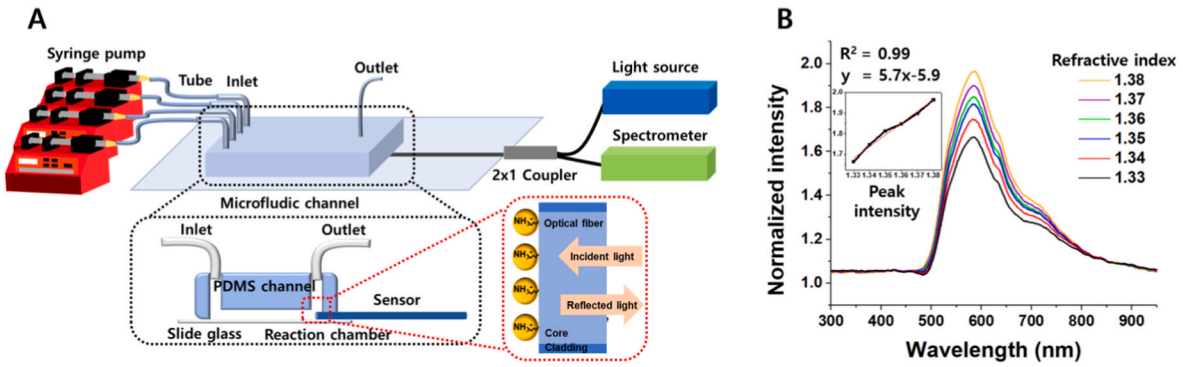

Fig. 2. Measurement configuration and sensor characteristics: (A) optical setup with fluid supply system, (B) spectrum variation according to refractive index in the FO LSPR sensor.

delivered to the microfluidic chip at a constant flow rate using a syringe pump (NE-300; New Era Pump System, USA). The optical properties of the proposed FO LSPR sensor combined with the microfluidic system, such as spectral shape, output intensity, and linearity of response, were confirmed. The spectra were sequentially monitored with an increase in the refractive index from 1.33 to 1.38 by steps of 0.01 (Fig. 2B). Refractive indices were adjusted through variable concentrations of glycerol in deionized (DI) water [46]. The resonance peak was observed at a typical position by the Au nanosphere, and the magnitude of the signal was sufficient for measurements compared to the noise of the detector [47]. As the refractive index increased, the sensor output also increased (based on the resonance peak), and the coefficient of determination (R^2) was 0.99, indicating a high correlation between the refractive index and the response of the FO LSPR sensor. Also, stability and reproducibility in different pHs were tested through repetitive measurements (Fig. S3).

2.4. Preparation of sandwich assay

Scheme 2 is a schematic sensorgram that demonstrates the expected changes in LSPR intensity during the preparation of the sandwich immunoassay and the antibody-antigen interactions based on the sandwich type. If the number of biomolecules adsorbed on Au is large, the refractive index increases, and the LSPR scale is proportional to this. The entire protocol for Tg detection was performed by injecting the samples into the microfluidic channel at a flow rate of 10 μL/min, which was adequate to induce the bioreactions with sufficient reactivity for short reaction times and to ensure the stability of the particles on a fiber-optic surface [48]. The sandwich-like immunoassay was prepared in five steps. First, to stabilize the signal, the baseline (I_0) was recorded for at least 5 min in a DI water atmosphere (stage 1 in Scheme 2). Second, 20 μg/mL of capture antibody in the PBS buffer was applied for 15 min for immobilization on the AuNP surface (stage 2 in Scheme 2). Anti-Tg antibodies are electrostatically adsorbed onto Au [49,50]. Third, all antibodies, except the bound antibodies, were adequately washed with DI water (stage 3 in Scheme 2). Fourth, to prevent the non-specific binding of antigens on the sensor surface, 1% BSA in the PBS buffer was reacted for 15 min (stage 4 in Scheme 2). In the final step, excess BSAs were removed in DI water to complete the preparation of the sandwich assay (stage 5 in Scheme 2).

The procedure for obtaining 2nd Ab-2nd AuNP conjugates for the magnification of LSPR responsivity by antibody-antigen reactions is as follows (the related pictures are displayed in Figs. S2A–C): first, the pH of the colloid of secondary AuNPs was modified to 9 by adding a 0.25 M potassium carbonate aqueous solution. Au colloid was characterized with transmission electron microscopy (Fig. S4D). The secondary AuNPs were prepared under the same conditions as those used for the fabrication of the FO LSPR sensor. Second, the colloid was blended (Thermomixer C, Eppendorf, Germany) with the detection antibodies for 30 min at 1400 rpm so that the final antibody concentration in the mixture was 1 μg/mL. Heavy aggregation occurred when the concentration of the anti-Tg antibody was higher than this value. Detection antibody-conjugated AuNPs were congregated (mySPIN12, Thermo Fisher Scientific, USA) at 10,000 rpm for 5 min and redispersed in the PBS buffer

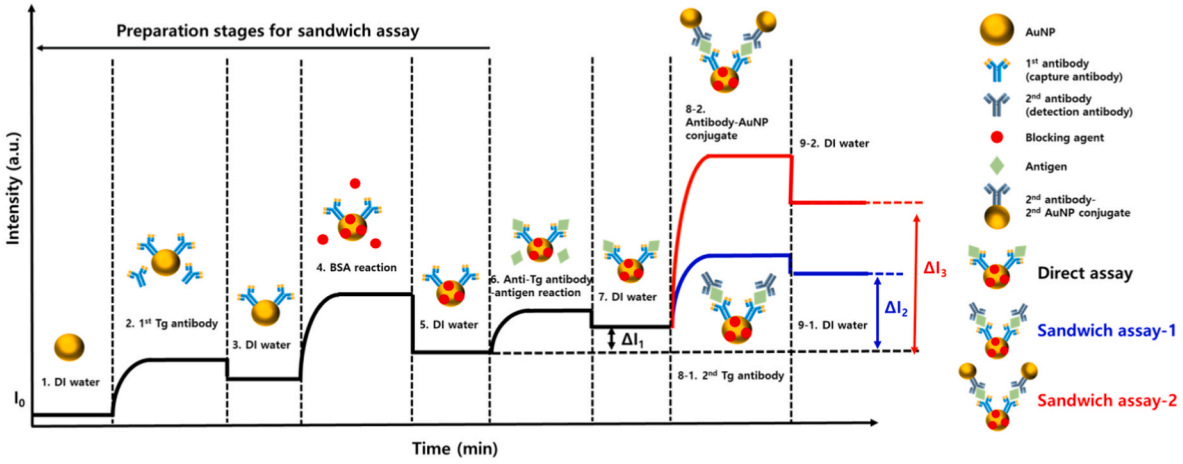

Scheme 2. Three protocols for the determination of the sensor output from the antibody-antigen reaction. Steps 1–5 are preparation processes for the immunoassay. Steps 6–7 are related to the direct assay. Steps 8-1–9-1 are for sandwich assay-1 using a 2nd antibody without the contribution of AuNP marker, and steps 8-2–9-2 are for sandwich assay-2 using 2nd Ab-2nd AuNP conjugates as a signal amplifier.

using bath sonication (Powersonic 440, Hwashin Technology, Republic of Korea). Finally, BSA was dissolved at a 1% level to block non-specific binding on the Au surface and shaken for 30 min. The resulting 2nd Ab-2nd AuNP conjugates were washed with PBS via centrifugation. Ultraviolet–visible spectra (UV1800, Shimadzu, Japan) measured in the wavelength range from 500 to 700 nm were compared in both conjugated and unconjugated Au colloids (Fig. S4).

2.5. Detection protocols of anti-Tg antibody-antigen interactions

To estimate the performance of the proposed FO LSPR biosensing system, Tg, a biomarker of differentiated thyroid cancer, was analyzed. Detection with the direct assay using capture anti-Tg antibodies, sandwich assay using only 2nd antibodies (sandwich assay-1), and sandwich assay using 2nd Ab-2nd AuNP conjugates (sandwich assay-2) was carried out. In the direct assay, the LSPR change due to the specific binding of Tg was defined as ΔI_1 in Scheme 2. After BSA treatment and rinsing of the sensor tip end, an antibody-antigen interaction was induced for 5 min (stage 6 in Scheme 2). Direct assay measurement was terminated by injecting DI water for cleaning (stage 7 in Scheme 2). In other words, the intensity difference between steps 7 and 5 (ΔI_1) was the output of the FO LSPR biosensor with a direct assay. The reason why the signal difference between washing processes was recorded with DI water is to gather the net change without the intervention of interfering species. In sandwich assay-1 using only 2nd antibodies without the incorporation of AuNPs, antigens were sandwiched by a 1 μg/mL detection antibody for 60 min (stage 8–1 in Scheme 2), and unbound antibodies were thoroughly flushed (stage 9–1 in Scheme 2). The response due to target recognition was determined as ΔI_2. The procedure for sandwich assay-2 assisted by antibody-functionalized AuNPs is as follows: after the completion of the direct assay (stage 7 in Scheme 2), 2nd Ab-2nd AuNP complexes were injected for 60 min to boost the output by the immunoassay (stage 8–2 in Scheme 2), and the unbound complexes were then removed (stage 9–2 in Scheme 2). The amplified LSPR change from the 2nd Ab-2nd AuNP compounds was expressed as ΔI_3. Figs. S2D and E are FE-SEM images of the fiber-optic cross-sections before and after sandwich assay-2, respectively. In fact, the number of nanoparticles increased with sandwich assay-2, and several coupled AuNPs were observed. The variations in the LSPR spectrum at 10 fg/mL Tg are shown in Fig. S3. The reaction time with the 2nd Ab-2nd AuNP conjugates was determined based on the saturation of the LSPR change with time (Fig. S4).

3. Result and discussion

3.1. Detection results of antibody-antigen interactions

Although the solution-process-based FO LSPR sensors are fabricated in the same batch, they have slightly different performances owing to differences in the size, density, and location of the nanoparticles fixed on the surface of each optical fiber. This can be explained by the variation in the output when sensors manufactured in one batch repeatedly measure the same concentration, which can reduce the uniformity and reliability of immunoassays. Previously, reproducibility was partially compensated by optimizing the size of the AuNPs. However, for further improvement, the deviation of the sensor outputs was moderated using a calibration method [51]. Calibration was applied by dividing $\Delta I_{1,\ 2,\ 3}$ by I_0 (Scheme 2). This technique enhances the reliability of the diagnosis results by using the relatively simple method of signal processing without the need for additional equipment. Fig. 3 shows the outputs of the FO LSPR sensor at various Tg concentrations using the three analysis methods. Identification was performed three times for each antigen level, and the molar concentrations were recorded together. The coefficient of variation (CV) was used to evaluate the distributions of the measured values. In our study, the measurable range of the proposed sensor was deemed above the concentration at which the mean of the measured values was greater than three times the standard deviation

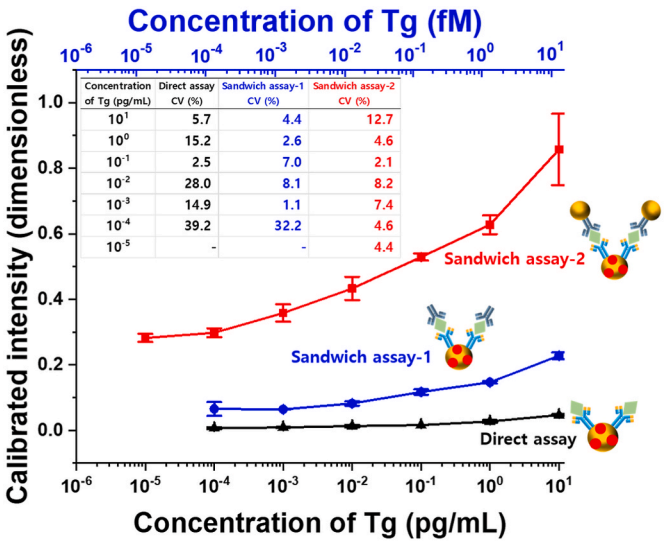

Fig. 3. Immunoassay results at various Tg levels from the direct assay (triangle), sandwich assay-1 using only detection antibodies (circle), and sandwich assay-2 with antibody-functionalized AuNPs (square).

(3SD) [52]. Therefore, levels with averages of less than 3SD were no longer measured. In the direct assay, a good reproducibility of 13.3% was observed on average, except for a CV of 39.2% at 100 ag/mL, where 3SD was above the mean of the measured values. Concentrations higher than 10 pg/mL were not determined because we aimed to compare the limit of detections (LODs) in the three immunoassay protocols. In sandwich assay-1, the measurable range was 1 fg/mL or greater, and a 4.64% CV was obtained, which is an improvement on the direct assay. This is assumed to be because the influence of signal amplification due to 2nd antibody binding is more dominant than the increase in the deviation of the measured values. In general, the CV can be lowered through surface texturing or tuning of the optical system; however, decline in the sandwich assay is due to the amelioration of the measuring protocol. In sandwich assay-2, excellent reproducibility was achieved, with an average CV of 6.27% at all concentrations. In addition, the proposed method allowed the detection of up to 10 ag/mL, which is one order of magnitude lower than that of the previous two methods. Measurable LSPR changes were monitored at 10 ag/mL; however, the diagnosis of lower concentrations was not attempted because the average of the responses was close to the noise of the optical system. LODs for the three strategies were acquired based on linear regression equations and 3SDs in the measurable ranges [53]. The FO LSPR sensor combined with the microfluidic chip had an LOD of 97.6 fg/mL (148 aM) with only a direct assay and without the support of the sandwich method, which was an improvement on previous research related to Tg detection [54,55]. The LOD of sandwich assay-1 was improved by approximately three times (32 fg/mL, 48 aM), which was attributed to the large shift in refractive index around the AuNPs due to the binding of the 2nd antibodies. Sandwich assay-2 using 2nd Ab-2nd AuNP conjugates achieved an LOD of 6.6 fg/mL (10 aM), which was fifteen times better than that of the direct assay. This is because of the high refractive index of the compounds, an increase in the number of AuNPs on the fiber-optic surface, and plasmonic coupling in the sandwiched structures [56]. At a concentration of 10 pg/mL, there was neither saturation of the calibrated intensity nor a sudden deterioration in CV; therefore, the dynamic range of the proposed method was expected to be larger than that measured in our study. As a result, we guaranteed an enhanced LOD by approximately several orders of magnitude compared to other high-sensitivity sensors (Table 1). These results prove that a signal amplification strategy aided by antibody-conjugated AuNPs is superior for improving biosensing performance. The developed technique can be advanced to a preventive tool to trace the recurrence of thyroid carcinoma through

Table 1
Comparison of detection limit of proposed method with developed Tg sensors.

Mechanism	Structure	LOD	References
Interferometry	Long period grating coated with tactic polystyrene	0.9 ng/mL	[57]
Colorimetry	Molecular imprinting polymer and graphene nanosheet composite	0.1 ng/mL	[58]
Electrochemistry	Polyvinylidene fluoride particle coated with streptavidins and AuNPs	15 pg/mL	[59]
Fluorometry	Tannylated ferritin nanocage	4.3 pg/mL	[60]
LSPR	Sandwich structure by 1st and 2nd AuNPs	6.6 fg/mL	This work

early monitoring of changes in low Tg levels.

3.2. Non-specific binding test

To confirm the tolerance of the non-specific binding of FO LSPR and the sandwich-type immunoassay, ferritin was mismatched to the anti-Tg capture antibody, and anti-Tg detection antibody-tagged AuNPs were sandwiched. We verified whether the proposed method yielded significant LSPR changes according to the concentration of ferritin from 1 fg/mL to 10 pg/mL. Fig. 4A shows the outputs of the Tg biosensor from immune reactions at various ferritin levels. Each point was identified in triplicate using an individual FO LSPR sensor. Because FO LSPR with anti-Tg antibodies and the blocking agent coating assures low non-specific binding to other biomarkers, no meaningful shifts in the LSPR intensity owing to ferritin binding were observed. This result indicates the reliability and specificity of the sandwich immunoassay using FO LSPR and 2nd Ab-2nd AuNP conjugates.

3.3. Patient's serum analyses

The serum is a complex biological medium that contains various molecules and proteins and has a normal pH of 7.4 for adult humans. Real samples with a complex matrix were surveyed to demonstrate the selectivity of the target biomarker and suitability of the proposed technique in a clinic. The performance was investigated by comparing Tg levels measured using radioimmunoassay (RIA, RIAKEY Thyroglobulin IRMA Tube, Shin Jin Medics, Republic of Korea) commercial kits and FO LSPR improved by antibody-functionalized AuNPs. The institutional review board of the National University Bundang Hospital approved this study and waived the need for individual informed consent (IRB no. B-1711/432–302). The patient's serum with 9.97 ng/mL of Tg was serially diluted to samples ranging from 0.997 fg/mL to 9.97 pg/mL (dilution from 1000-fold to 10 million times). The Tg concentrations in the proposed method were deduced by linearly fitting the standard curve of Fig. 3 and substituting the LSPR differences obtained in the real samples. In Fig. 4B, the x-axis represents the Tg levels measured using the RIA kit and the y-axis shows those from the developed sensor. The correlation between the two variables was validated with linear function fitting, and a similar performance was observed with the R^2 of 0.99 and slope of 1.09 between the two devices. Large CV at the lowest level (below the LOD of the proposed sensor) was affected by an increase in the dilution factor, and the average CV excluding it was reasonable at 13.9% [61,62]. The slight increase in CV was due to various interfering species in the serum. CVs were acquired through three repetitions at each concentration. Degradations also accumulated during the process of converting the measured values into concentrations. The sandwich-type FO LSPR immunosensor suggested the potential for clinical application.

4. Conclusion

The paradigm of medical services is changing from a treatment-centered approach to a prevention-centered approach. Therefore, the need for a highly sensitive biosensor to secure public safety through disease prevention by early detection has become more important. In this study, we aimed to achieve high-sensitivity measurements using an LSPR sensor, a representative real-time biosensing technology with a relatively well-established principle. An FO LSPR sensor with ease of handling, portability, low cost, and long-range controllability was fabricated by immobilizing AuNPs in a fiber-optic cross-section. A sandwich scenario based on 2nd Ab-2nd AuNP conjugates was applied, which amplified the response in biomarker recognition through the increased density of AuNPs and the coupling between them. In particular, in the proposed approach with a signal amplifier, the LOD was improved by approximately fifteen times (6.6 fg/mL, 10 aM) compared with the case without the sandwich structure. This was the result of a large LSPR change from the increase in density and plasmonic coupling by nanoparticle adsorption. Selectivity was explored using the control antigen, which had no affinity for the applied capture and detection antibodies. The Tg in the serum matrix was analyzed and compared using our sandwich-type FO LSPR immunosensor and the clinically used RIA kit, and the two devices showed a strong correspondence. The results revealed that the proposed sensor is as specific and sensitive as a commercial kit in a partially rapid manner. The developed method is expected to be expanded as a tool to enable the early treatment of various diseases by detecting biomarkers that are present in small quantities in the body. The adoption of high-functionality nanoparticles engineered in shape and material will guide further improvements of biosensors aiming for ultrasensitivity.

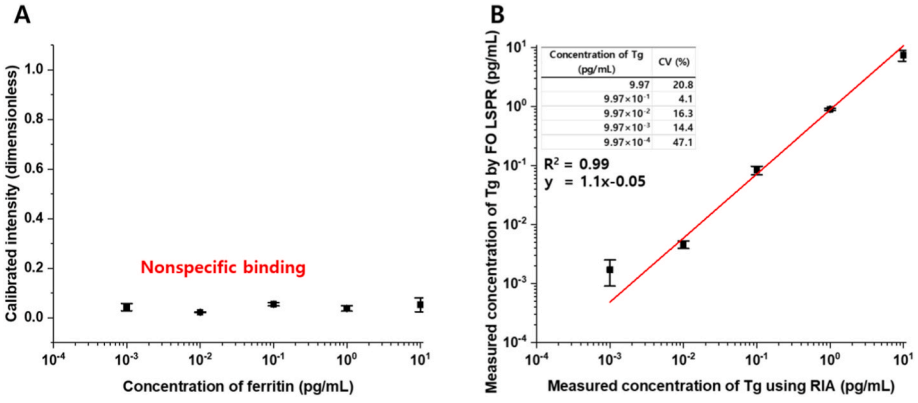

Fig. 4. Specificity of the proposed method, and performance comparison with the commercial kit. (A) Selectivity certification of the FO LSPR biosensor, (B) correlation between the RIA tool used in the field and the proposed sensor based on real sample analyses.

CRediT authorship contribution statement

Hyeong-Min Kim: Conceptualization, Methodology, Validation, Investigation, Data curation, and, Writing – original draft. **Hyo-Jun Kim:** Validation, Investigation, and, Data curation. **Jae-Hyoung Park:** Supervision, Resources, and, Project administration. **Seung-Ki Lee:** Term, Conceptualization, Methodology, Writing – review & editing, Supervision, Resources, and, Project administration.

Declaration of competing interest

The authors declare that they have no known competing financial interests or personal relationships that could have influenced the work reported in this paper.

Acknowledgment

This work was supported by a National Research Foundation of Korea (NRF) grant funded by the Korean government (MSIT) (No. NRF-2021M3C1C3097205). The authors thank Prof. Ho-Young Lee of the Department of Nuclear Medicine, Seoul National University Bundang Hospital for his contribution and characterization of the biosample.

Appendix A. Supplementary data

Supplementary data to this article can be found online at https://doi.org/10.1016/j.aca.2022.339960.

References

[1] R.V. Devi, M. Doble, R.S. Verma, Nanomaterials for early detection of cancer biomarker with special emphasis on gold nanoparticles in immunoassays/sensors, Biosens. Bioelectron. 68 (2015) 688–698.
[2] S. Kumar, R. Singh, Recent optical sensing technologies for the detection of various biomolecules, Opt Laser. Technol. 134 (2021), 106620.
[3] N.S. Heo, C.H. Kwak, H. Lee, D. Kim, S. Lee, G.B. Kim, S. Kwon, W.S. Kim, Y.S. Huh, Simple diagnosis of HbA1c using the dual-plasmonic platform integrated with LSPR and SERS, J. Cryst. Growth 469 (2017) 154–159.
[4] Y.H. Wang, K.J. Huang, X. Wu, Recent advances in transition-metal dichalcogenides based electrochemical biosensors: a review, Biosens. Bioelectron. 97 (2017) 305–316.
[5] S.K. Krishnan, E. Singh, P. Singh, M. Meyyappan, H.S. Nalwa, A review on graphene-based nanocomposites for electrochemical and fluorescent biosensors, RSC Adv. 9 (2019) 8778–8881.
[6] A. Thapa, A.C. Soares, J.C. Soares, I.T. Awan, D. Volpati, M.E. Melendez, J.H.T. G. Fregnani, A.L. Carvalho, O.N. Oliveira Jr., Carbon nanotube matrix for highly sensitive biosensors to detect pancreatic cancer biomarker CA19-9, ACS Appl. Mater. Interfaces 9 (2017) 25878–25886.
[7] E.A. Songa, J.O. Okonkwo, Recent approaches to improving selectivity and sensitivity of enzyme-based biosensors for organophosphorus pesticides: a review, Talanta 155 (2016) 289–304.
[8] L. Zhao, H. Li, J. Meng, A.C. Wang, P. Tan, Y. Zou, Z. Yuan, J. Lu, C. Pan, Y. Fan, Y. Zhang, Z.L. Wang, Z. Li, Reversible conversion between Schottky and ohmic contacts for highly sensitive, multifunctional biosensors, Adv. Funct. Mater. 30 (2020), 1907999.
[9] R. Funari, N. Bhalla, K.Y. Chu, B. Soderstrom, A.Q. Shen, Nanoplasmonics for real-time and label-free monitoring of microbial biofilm formation, ACS Sens. 3 (2018) 1499–1509.
[10] L. Singh, R. Singh, B. Zhang, S. Cheng, B.K. Kaushik, S. Kumar, LSPR based uric acid sensor using graphene oxide and gold nanoparticles functionalized tapered fiber, Opt. Fiber Technol. 53 (2019), 102043.
[11] G. Zhu, N. Agrawal, R. Singh, S. Kumar, B. Zhang, C. Saha, C. Kumar, A novel periodically tapered structure-based gold nanoparticles and graphene oxide–Immobilized optical fiber sensor to detect ascorbic acid, Opt Laser. Technol. 127 (2020), 106156.
[12] J.M. Haber, P.R.C. Gascoyne, K. Sokolov, Rapid real-time recirculating PCR using localized surface plasmon resonance (LSPR) and piezo-electric pumping, Lab Chip 17 (2017) 2821–2830.
[13] F. Fernández, O. Garcia-Lopez, E. Tellechea, A.C. Asensio, I. Cornago, LSPR cuvette for real-time biosensing by using a common spectrophotometer, IEEE Sensor. J. 16 (2016) 4158–4165.
[14] N. Agrawal, C. Saha, C. Kumar, R. Singh, B. Zhang, S. Kumar, Development of uric acid sensor using copper oxide and silver nanoparticles immobilized SMSMS fiber structure-based probe, IEEE Trans. Instrum. Meas. 69 (2020) 9097–9104.
[15] L. Singh, G. Zhu, R. Singh, B. Zhang, W. Wang, B.K. Kaushik, S. Kumar, Gold nanoparticles and uricase functionalized tapered fiber sensor for uric acid detection, IEEE Sensor. J. 20 (2019) 219–226.
[16] D.K. Pattadar, J.N. Sharma, B.P. Mainali, F.P. Zamborini, Impact of the assembly method on the surface area-to-volume ratio and electrochemical oxidation potential of metal nanospheres, J. Phys. Chem. C 123 (2019) 24304–24312.
[17] O. Adegoke, M.A. Pereira-Barros, S. Zolotovskaya, A. Abdolvand, N.N. Daeid, Aptamer-based cocaine assay using a nanohybrid composed of ZnS/Ag_2Se quantum dots, graphene oxide and gold nanoparticles as a fluorescent probe, Microchim. Acta 187 (2020) 1–12.
[18] D. Paul, S. Dutta, R. Biswas, LSPR enhanced gasoline sensing with a U-bent optical fiber, J. Phys. D Appl. Phys. 49 (2016), 305104.
[19] K. Sadani, P. Nag, S. Mukherji, LSPR based optical fiber sensor with chitosan capped gold nanoparticles on BSA for trace detection of Hg (II) in water, soil and food samples, Biosens. Bioelectron. 134 (2019) 90–96.
[20] E. Klantsataya, P. Jia, H. Ebendorff-Heidepriem, T.M. Monro, A. François, Plasmonic fiber optic refractometric sensors: from conventional architectures to recent design trends, Sensors 17 (2017) 12.
[21] A.K. Sharma, A.K. Pandey, B. Kaur, A review of advancements (2007–2017) in plasmonics-based optical fiber sensors, Opt. Fiber Technol. 43 (2018) 20–34.
[22] O. Adegoke, N.N. Daeid, Alloyed AuFeZnSe quantum dots@gold nanorod nanocomposite as an ultrasensitive and selective plasmon-amplified fluorescence OFF-ON aptasensor for arsenic (III), J. Photochem. Photobiol. Chem. 426 (2022), 113755.
[23] K. Shah, P. Maghsoudlou, Enzyme-linked immunosorbent assay (ELISA): the basics, Br. J. Hosp. Med. 77 (2016) C98–C101.
[24] S. Kim, H.J. Lee, Direct detection of α-1 antitrypsin in serum samples using surface plasmon resonance with a new aptamer–antibody sandwich assay, Anal. Chem. 87 (2015) 7235–7240.
[25] X. Fu, L. Chen, J. Choo, Optical nanoprobes for ultrasensitive immunoassay, Anal. Chem. 89 (2017) 124–137.
[26] X. Ma, S. He, B. Qiu, F. Luo, L. Guo, Z. Lin, Noble metal nanoparticle-based multicolor immunoassays: an approach toward visual quantification of the analytes with the naked eye, ACS Sens. 4 (2019) 782–791.
[27] K. Karn-Orachai, K. Sakamoto, R. Laocharoensuk, S. Bamrungsap, T. Dharakul, K. Miki, SERS-based immunoassay on 2D-arrays of Au@Ag core–shell nanoparticles: influence of the sizes of the SERS probe and sandwich immunocomplex on the sensitivity, RSC Adv. 7 (2017) 14099–14106.
[28] M.A. Pereira-Barros, N.N. Daeid, O. Adegoke, Rapid and selective aptamer-based fluorescence detection of salivary lysozyme using plasmonic metal-enhanced fluorescence of ZnSSe alloyed quantum dots-gold nanoparticle nanohybrid, J. Photochem. Photobiol. Chem. 418 (2021), 113384.
[29] W. Zheng, X. Jiang, Integration of nanomaterials for colorimetric immunoassays with improved performance: a functional perspective, Analyst 141 (2016) 1196–1208.
[30] O. Adegoke, S. Zolotovskaya, A. Abdolvand, N.N. Daeid, Rapid and highly selective colorimetric detection of nitrite based on the catalytic-enhanced reaction of mimetic Au nanoparticle-CeO_2 nanoparticle-graphene oxide hybrid nanozyme, Talanta 224 (2021), 121875.
[31] O. Yavas, M. Svedendahl, P. Dobosz, V. Sanz, R. Quidant, On-a-chip biosensing based on all-dielectric nanoresonators, Nano Lett. 17 (2017) 4421–4426.
[32] Y. Chen, J. Liu, Z. Yang, J.S. Wilkinson, X. Zhou, Optical biosensors based on refractometric sensing schemes: a review, Biosens. Bioelectron. 144 (2019), 111693.
[33] Y. Xu, Z. Zhang, R.M. Yi, X.D. Guo, Z.M. Qi, Single-layer graphene-based surface plasmon resonance sensor with dynamic evanescent field enhancement for biomarker study, J. Mod. Opt. 67 (2020) 671–681.
[34] H.Y. Song, T.I. Wong, A. Sadovoy, L. Wu, P. Bai, J. Deng, S. Guo, Y. Wang, W. Knoll, X. Zhou, Imprinted gold 2D nanoarray for highly sensitive and convenient PSA detection via plasmon excited quantum dots, Lab Chip 15 (2015) 253–263.
[35] S. Kim, H.J. Lee, Gold nanostar enhanced surface plasmon resonance detection of an antibiotic at attomolar concentrations via an aptamer-antibody sandwich assay, Anal. Chem. 89 (2017) 6624–6630.
[36] O. Adegoke, N.N. Daeid, Polymeric-coated Fe-doped ceria/gold hybrid nanocomposite as an aptasensor for the catalytic enhanced colorimetric detection of 2, 4-dinitrophenol, Colloids Surf. A Physicochem. Eng. Asp. 627 (2021), 127194.
[37] Y. Wang, G. Zhu, M. Li, R. Singh, C. Marques, R. Min, B.K. Kaushik, B. Zhang, R. Jha, S. Kumar, Water pollutants p-Cresol detection based on Au-ZnO nanoparticles modified tapered optical fiber, IEEE Trans. NanoBioscience 20 (2021) 377–384.
[38] F. Nasrin, A.D. Chowdhury, K. Takemura, I. Kozaki, H. Honda, O. Adegoke, E. Y. Park, Fluorometric virus detection platform using quantum dots-gold nanocomposites optimizing the linker length variation, Anal. Chim. Acta 1109 (2020) 148–157.
[39] O. Adegoke, C. McKenzie, N.N. Daeid, Multi-shaped cationic gold nanoparticle-L-cysteine-ZnSeS quantum dots hybrid nanozyme as an intrinsic peroxidase mimic for the rapid colorimetric detection of cocaine, Sensor. Actuator. B Chem. 287 (2019) 416–427.
[40] J. Kim, S.Y. Oh, S. Shukla, S.B. Hong, N.S. Heo, V.K. Bajpai, H.S. Chun, C.H. Jo, B. G. Choi, Y.S. Huh, Y.K. Han, Heteroassembled gold nanoparticles with sandwich-immunoassay LSPR chip format for rapid and sensitive detection of hepatitis B virus surface antigen (HBsAg), Biosens. Bioelectron. 107 (2018) 118–122.
[41] D.S. Wang, S.K. Fan, Microfluidic surface plasmon resonance sensors: from principles to point-of-care applications, Sensors 16 (2016) 1175.
[42] J. Chen, S. Shi, R. Su, W. Qi, R. Huang, M. Wang, L. Wang, Z. He, Optimization and application of reflective LSPR optical fiber biosensors based on silver nanoparticles, Sensors 15 (2015) 12205–12217.

[43] H.H. Jeong, N. Erdene, J.H. Park, D.H. Jeong, S.K. Lee, Analysis of fiber-optic localized surface plasmon resonance sensor by controlling formation of gold nanoparticles and its bio-application, J. Nanosci. Nanotechnol. 12 (2012) 7815–7821.
[44] N. Agrawal, B. Zhang, C. Saha, C. Kumar, X. Pu, S. Kumar, Ultra-sensitive cholesterol sensor using gold and zinc-oxide nanoparticles immobilized core mismatch MPM/SPS probe, J. Lightwave Technol. 38 (2020) 2523–2529.
[45] H.M. Kim, D.H. Jeong, H.Y. Lee, J.H. Park, S.K. Lee, Design and validation of fiber optic localized surface plasmon resonance sensor for thyroglobulin immunoassay with high sensitivity and rapid detection, Sci. Rep. 11 (2021) 1–9.
[46] K. Lodewijks, W. Van Roy, G. Borghs, L. Lagae, P. Van Dorpe, Boosting the figure-of-merit of LSPR-based refractive index sensing by phase-sensitive measurements, Nano Lett. 12 (2012) 1655–1659.
[47] M. Chauhan, V.K. Singh, Review on recent experimental SPR/LSPR based fiber optic analyte sensors, Opt. Fiber Technol. 64 (2021), 102580.
[48] N.V. Zaytseva, V.N. Goral, R.A. Montagna, A.J. Baeumner, Development of a microfluidic biosensor module for pathogen detection, Lab Chip 5 (2005) 805–811.
[49] W.P. Hall, S.N. Ngatia, R.P. Van Duyne, LSPR biosensor signal enhancement using nanoparticle−antibody conjugates, J. Phys. Chem. C 115 (2011) 1410–1414.
[50] A. Salahvarzi, M. Mahani, M. Torkzadeh-Mahani, R. Alizadeh, Localized surface plasmon resonance based gold nanobiosensor: determination of thyroid stimulating hormone, Anal. Biochem. 516 (2017) 1–5.
[51] H.M. Kim, J.H. Park, D.H. Jeong, H.Y. Lee, S.K. Lee, Real-time detection of prostate-specific antigens using a highly reliable fiber-optic localized surface plasmon resonance sensor combined with micro fluidic channel, Sensor. Actuator. B Chem. 273 (2018) 891–898.
[52] J. Mocak, A.M. Bond, S. Mitchell, G. Scollary, A statistical overview of standard (IUPAC and ACS) and new procedures for determining the limits of detection and quantification: application to voltammetric and stripping techniques (technical report), Pure Appl. Chem. 69 (1997) 297–328.
[53] H.M. Kim, D.H. Jeong, H.Y. Lee, J.H. Park, S.K. Lee, Improved stability of gold nanoparticles on the optical fiber and their application to refractive index sensor based on localized surface plasmon resonance, Opt Laser. Technol. 114 (2019) 171–178.
[54] S. Choi, J. Chae, A microfluidic biosensor based on competitive protein adsorption for thyroglobulin detection, Biosens. Bioelectron. 25 (2009) 118–123.
[55] C. Spencer, I. Petrovic, S. Fatemi, Current thyroglobulin autoantibody (TgAb) assays often fail to detect interfering TgAb that can result in the reporting of falsely low/undetectable serum Tg IMA values for patients with differentiated thyroid cancer, J. Clin. Endocrinol. Metab. 96 (2011) 1283–1291.
[56] S.H. Baek, H.W. Song, S. Lee, J.E. Kim, Y.H. Kim, J.S. Wi, J.G. Ok, J.S. Park, S. Hong, M.K. Kwak, H.J. Lee, S.W. Nam, Gold nanoparticle-enhanced and roll-to-roll nanoimprinted LSPR platform for detecting interleukin-10, Front. Chem. 8 (2020) 285.
[57] G. Quero, M. Consales, R. Severino, P. Vaiano, A. Boniello, A. Sandomenico, M. Ruvo, A. Borriello, L. Diodato, S. Zuppolini, M. Giordano, I.C. Nettore, C. Mazzarella, A. Colao, P.E. Macchia, F. Santorelli, A. Cutolo, A. Cusano, Long period fiber grating nano-optrode for cancer biomarker detection, Biosens. Bioelectron. 80 (2016) 590–600.
[58] X. Wang, K. Huang, H. Cui, H. Zhang, L. Zeng, Y. Zhou, T. Jing, Label-free determination of thyroglobulin using template-probe double imprinted composites, Sensor. Actuator. B Chem. 313 (2020), 128028.
[59] M.O.S. de Moraes, J.D.D.P. de Moraes, M.M. da Silva Paula, M.G.F. Sales, W. R. Brito, Highly sensitive electrochemical immunosensor using a protein-polyvinylidene fluoride nanocomposite for human thyroglobulin, Bioelectrochemistry 142 (2021), 107888.
[60] E. Turan, F. Şahin, Z. Suludere, H. Tümtürk, A fluoroimmunodiagnostic nanoplatform for thyroglobulin detection based on fluorescence quenching signal, Sensor. Actuator. B Chem. 300 (2019), 127052.
[61] L. Guo, G. Chen, D.H. Kim, Three-dimensionally assembled gold nanostructures for plasmonic biosensors, Anal. Chem. 82 (2010) 5147–5153.
[62] X. Wang, Y. Li, H. Wang, Q. Fu, J. Peng, Y. Wang, J. Du, Y. Zhou, L. Zhan, Gold nanorod-based localized surface plasmon resonance biosensor for sensitive detection of hepatitis B virus in buffer, blood serum and plasma, Biosens. Bioelectron. 26 (2010) 404–410.